Reliability Engineering and Resilience 2-2 (2020) 01-16

Contents lists available at **RER**

Reliability Engineering and Resilience

Journal homepage: www.rengrj.com

Derrick-Supported Flare-Stacks Seismic Fragility Assessment: A Case Study

B. SayyafZadeh, S. Kouhestani, M. Sharifi

Department of Civil Engineering, Faculty of Engineering, University of Qom, Qom, Iran
Corresponding author: *m.sharifi@qom.ac.ir*

https://doi.org/10.22115/RER.2021.283929.1040

ARTICLE INFO

Article history:
Received: 01 May 2021
Revised: 19 June 2021
Accepted: 25 August 2021

Keywords:
Incremental dynamic analysis;
Flare;
Fragility curve;
Seismic vulnerability;
Probabilistic assessment.

ABSTRACT

Today oil, gas and petrochemical plants risk mitigation and management due to various aspects such as energy supply, financial implications, life loss and repairs has become a primary concern. One of the approaches that can be used for risk assessment of such these plants which are composed of different types of equipment and structures that have different responses and consequences is the probabilistic analysis. Flare is a process equipment that is widely used in oil, gas and petrochemical plants and depending on the height and type of lateral stability is categorized into self-supported, guy-supported and derrick-supported. In this article seismic behavior of a derrick-supported flare is investigated using finite element method and incremental dynamic analysis as a case study. For this purpose, various limit states were considered and for each of them a fragility curve is calculated and also presented with statistical parameters. The results showed that in ordinary seismic intensities there is no significant seismic demand on the investigated structure but in the range of rare intensities that can trigger technological disasters, there is probability of failure and consequently escalating the disaster.

1. Introduction

The development of the oil and gas industry, its role in ensuring global energy security and the increased need for petrochemical products has been a focus of much attention. However, the

How to cite this article: SayyafZadeh B, Kouhestani S, Sharifi M. Derrick-supported flare-stacks seismic fragility assessment: a case study. Reliab. Eng. Resil. 2020;2(2):01–20. https://doi.org/10.22115/RER.2021.283929.1040

growth of this industry has been accompanied by challenges such as the consequences of an earthquake. The construction of industrial plants in areas with a potential earthquake hazard is widespread, which makes seismic hazard assessment of these plants a necessity. Choosing the right location on which to build a plant is a strategic choice that should minimize the cost of transport of the product through pipelines. As a result, factories are moving closer to urban areas. Controlling of an Event is lost when a non-structural or structural member fails and endangers human lives with catastrophic environmental and financial consequences [1].

Earthquakes are natural hazards that have caused significant damage to many industrial sites. However, national and international standards do not provide procedures for assessment of the overall risk to industrial plants located in earthquake-prone areas [2]. The 2011 Tohoku earthquake and tsunami triggered the Fukushima nuclear power plant disaster. The 1999 Kocaeli earthquake in Turkey and 2008 Wenchuan earthquake in China are additional examples of natural disasters that demonstrate that systematic risk assessment of seismic events is necessary for industrial plants [3].

Oil and gas and petrochemical refineries typically include equipment as well as structural and non-structural structures. Cylindrical tanks and horizontal pressure vessels are examples of common non-structural structures. These are commonly used for storing water, petroleum, chemicals and natural gas. There have been many seismic evaluations of such equipment. Eidinger [4] provided seismic fragility functions for non-structural components in an industrial joint facility. Danesi [5] used incremental dynamic analysis (IDA) and fragility functions on a case study of a petrochemical pipe rack in the Caribbean. Bursi et al. [6] carried out seismic analysis of the performance of petrochemical piping systems as a case study.

A major non-structural component of an oil plant is the flares. Factors such as power outages, changes in feed input to sections, exceeding the design capacity of production units, improper maintenance, deviation from correct methods and operating instructions and human error can cause pressure changes in tanks, towers and other industrial equipment [7]. Pressure changes, in turn, can cause irreparable damage to industrial equipment and sometimes result in casualties. Flares are one of the most important ways of protecting industrial devices against overpressure.

Flares are stacks in which organic matter and combustible gases are burned at a distance from the plant before they cause a problem for the facility. For oilfields and wells, refineries, petrochemical and chemical plants, they are designed to protect equipment and workers from heat radiation from combustion gases as well as to remove harmful and toxic gases from the industrial environment. Thus, a flare is a safety device that protects a factory from the consequences of excess gas [8].

Generally, flares used in refineries can be either elevated or ground flares. An elevated flare is designed for maximum combustible material flow and maximum permissible combustion radiation. The types of stacks include self-supported, guy-supported and derrick-supported [9], as shown in Fig**. 1**.

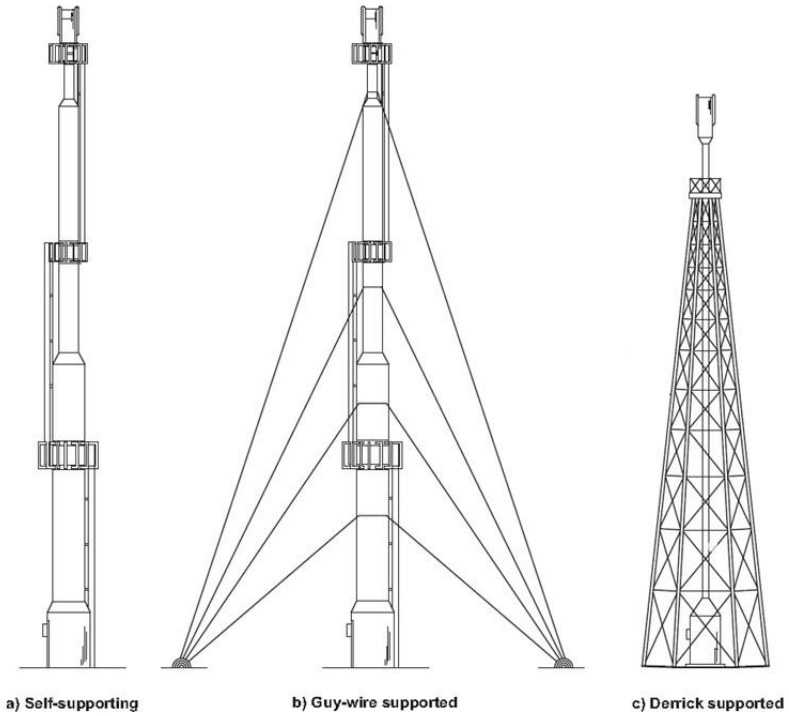

Fig. 1. Flare Types.

The diameter and wall thickness required for a stack will increase with an increase in its height or the wind loading [10]; however, as the flare height and/or wind loading increases, the diameter and wall thickness required will increase the expense of construction. Self-supported stacks are the simplest and most economical design for applications requiring short-stack heights (30-100 ft).

The easiest of all the support methods to control lateral forces is the guy-supported flare. Normally, sets of three wires placed 120° apart are anchored at various elevations. This requires a considerable amount of land because the guy wires must be spread apart. As a rule of thumb, space required to erect a guy-supported flare is a circle on the ground with a radius equal to the height of the flare stack [11].

Derrick-supported flares can be built as high as required because the system load is spread over the derrick structure and it will no longer relate to an increase in the diameter of the flare pipe [12]. Failure of these types of structures after an earthquake are seldom reported. One of the few reports is for the 2008 earthquake in Wenchuan, China (7.9 magnitude; depth of 19 km; PGA = 0.96 g). Observations

indicated that some members of a flare with a metal truss buckled under pressure and the entire flare system bent; however, it continued to operate. In that region, structures have been designed to withstand PGA = 0.22g [13], indicating that the seismic effects on these structures were low.

The current study is a probabilistic seismic evaluation of derrick-supported flares. A case study of an actual flare was modeled using the finite element method and analyzed by IDA. Then,

considering the different limit states of the structures, the results of the IDA were used to produce fracture curves.

2. IDA method

IDA has been adopted by the US Federal Emergency Management Agency (FEMA) to determine the global collapse capacity. The concept was first expressed by Bertero (1977) and IDA was developed by Cornell et al.[14]. This method evaluates the seismic response of a structure by taking into account the inherent uncertainty of earthquakes. Because it considers the behavior of materials to be nonlinear as well as dynamic in nature, it is the most accurate method for estimating the behavior of structures.

IDA consists of a set of nonlinear time-history analyses that determine the amount of damage in terms of earthquake intensity. Each record is scaled to cover an appropriate range of seismic intensity as well as structural behavior from a linearly elastic state to collapse [15].

To perform IDA, the seismic intensity parameter is first scaled, beginning with a very small value, to obtain the elastic behavior under to a certain level of seismic intensity to reach the desired failure limit with the use of a suitable algorithm. The structure is dynamically analyzed using an earthquake record and the time scales. At the end of each analysis step, the damage intensity corresponding to the seismic intensity level is recorded. For each scaled record, a response-intensity curve, called an IDA single record, is obtained. The indices and the earthquake scale factor are defined below.

2.1. Seismic intensity measure

The seismic intensity measure (IM) is a scalable quantity and a function of the main accelerogram which changes as the accelerogram increases or decreases. Examples of scalable IMs are peak ground acceleration (PGA), peak ground velocity (PGV) and the 5% damped first-mode spectral acceleration (Sa(T1;5%)). The seismic IM incorporates the dynamic properties of a record and its proper selection reduces the dispersion of data [15]. In the current study, PGA was selected as the seismic IM.

2.2. Damage intensity measure

The damage measure (DM) is a positive scalar quantity that characterizes the response of the structural model in response to seismic loading and is deduced from the output of the corresponding nonlinear dynamic analysis [15]. The choice of an appropriate measure depends largely on the application, the type of structure, its importance and the purpose of the analysis. The maximum intersegment displacement ratio ($ISDR_{max}$) is a proper criterion for estimating DM and, in this study, this value was considered to be the engineering demand parameter (EDP) [16].

2.3. Scale factor

The scale factor (SF) is a positive number (such as λ) with a range from zero to infinity. Multiplying this value by the initial accelerogram values will produce a scaled accelerometer.

Depending on the value of λ (λ > 1 or λ < 1), the intensity will decrease or increase. A value of λ = 1 represents a natural accelerogram.

Initially, a very small value (e.g. 0.005g) is selected to measure the seismic intensity for the IM parameter that will guarantee a linear response by the structure. Then, using a constant coefficient, the seismic intensity is increased incrementally. The scale coefficient in each step can be calculated as:

$$SF = \frac{PGA(i)}{PGA} \quad (1)$$

where PGA is the peak ground acceleration and PGA(i) is the value of seismic intensity considered in this study (0.1, 0.2, …, 3).

Each IDA curve for each acceleration reflects the behavior of the structure under a particular earthquake record and cannot be generalized to all records; thus it cannot predict the behavior of the structure for a specific earthquake. It is necessary to include a sufficient number of accelerograms to encompass a complete range of structural responses in order to arrive at an accurate estimate of structural behavior. This results in the creation of multi-record IDA curves. To reduce the dispersion of information and allow exanimation of the curves, it is essential to summarize the data for how the structure responds at each level of demand and achieve a general state of structural behavior.

In this case, each curve becomes a random function of DM = f (IM). Taking into account the damage values determined at each level of earthquake intensity produces 50%, 16% and 84% of the response spectra. The 50% statistic represents the average of the spectral acceleration values. By specifying the desired failure modes, it is possible to investigate the performance and behavior of structures under different earthquake records and evaluate the seismic demand of the structures [15].

3. Fragility curves

An earthquake is random in nature; thus, it should be considered using a probabilistic approach. Instead of expressing the seismic intensity that brings the structure to a particular level of performance, the probability of reaching that level or exceeding the EDP for different earthquake intensities is expressed. Such curves are called the fragility curves and can be expressed as:

$$F_i(im) = P(EDP \geq d_i | IM = im) \quad (2)$$

where Fi(im) is the probability of reaching or exceeding the EDP as expressed by the damage index (DI) at seismic intensity IM = im. The following steps should be taken to obtain a fragility curve:

- Introduce the limit-states.
- Form the response matrix, which is the damage index for the seismic index.
- Use statistical analysis to extract the fragility curves.
- Simplify the fragility curves for easier application.

3.1. Performance levels

Limit states can be considered as the point of deformation of a structure. In the present study, the probability function values for each structure and for each earthquake intensity as calculated by the maximum intersegment displacement ratio (ISDRmax) exceeded the level in Table 1 based on FEMA 365 (Asce et al. 2000) standard C1-3.

Table 1
Performance Levels.

Limit state	Drift
Immediate occupancy (IO)	0.005
Life safety (LS)	0.015
Collapse prevention (CP)	0.02

3.2. Response matrix

The response matrix is formulated using IDA and the earthquake record scale at specified times to reach the level of failure and then extracting the structural responses as the number of accelerations multiplied by the number of scaled IM levels. As stated, the seismic intensity is equal to the PGA and the extracted damage index is the intersegment displacement ratio. For each column in the matrix (for the same PGA), the displacement responses can be further considered as a lognormal distribution with a probability density function (PDF) as follows:

$$f_x(x) = \frac{1}{\sqrt{2\pi}\zeta x} exp\left(-\frac{1}{2}\left(\frac{ln(x)-\lambda}{\zeta}\right)^2\right) \quad (3)$$

where ζ and λ are the lognormal distribution of random displacement parameters for variable x. The data from these parameters for a normal distribution can be used to calculate the mean and standard deviation. Mean μ and standard deviation σ of the sample population are:

$$\lambda = ln\,\mu - \frac{1}{2}\zeta^2 \quad (4)$$

$$\zeta^2 = ln[1+\delta^2] \quad (5)$$

$$\delta = \frac{\sigma}{\mu} \quad (6)$$

3.3. Fragility analysis

In accordance with the drift bound of each defined damage state, the fragility curve for damage state S_i is the conditional probability at which the damage state of the flare exceeds S_i at a specific PGA value. This definition can be expressed as:

$$P(S > s|PGA) = P(X > x_i|PGA) = 1 - \varphi\left[\frac{ln(x_i)-\lambda}{\zeta}\right] \quad (7)$$

where ϕ is the standard normal cumulative distribution function and x_i is the upper bound for S_i $(I, II, III = i)$.

3.4. Simplified fragility curve

A fragility curve is frequently expressed as a lognormal cumulative distribution function (CDF). In this way, it can be represented using only two parameters as follows:

$$F_A(a) = \int_0^a \frac{1}{\sqrt{2\pi}\zeta_A a} exp\left(-\frac{1}{2}\left(\frac{ln(a)-ln(m_a)}{\zeta_A}\right)^2\right) da \quad (8)$$

where A is the random variable of the PGA and m_A is the median of A (ξ_A) and is the logarithmic standard deviation of A. Eq. (8) can be related to the standard normal cumulative distribution function using argument Z as follows:

$$F_A(a) = \phi[z] \tag{9}$$

where Z is the standard normal variable, which is defined as $Z = [ln\,(a) - ln\,(m_A)] \,/\, \zeta_A$ on the fragility curve. As the standard normal variable of the fragility curve at a PGA of a for fragility probability $F_A(a)$ at a, the normal variable can be calculated as:

$$z = \phi^{-1}[F_A(a)] \tag{10}$$

where $\phi^{-1}(0)$ is the inverse function of the standard normal cumulative distribution.

When describing a standard normal variable, the relationship of Z versus $ln(a)$ is linear for a fragility curve with a lognormal distribution .The intercept and slope of the linear relation will be $ln(m_A)$ and ξ_A, respectively. Accordingly, for a fragility curve to fit the lognormal cumulative distribution function, the previous argument can be used. First, for each fragility curve, Z is the standard normal variable with associated fragility probabilities for all of PGA values (Eq. (10)). Then, the relationship of Z versus $ln(a)$ can be constructed to retrieve the values of $ln(m_A)$ and ξ_A [17].

4. Modeling and assumptions

In the present study, the seismic vulnerability of one flare with a height of 46 m (denoted as GOSP) in Khuzestan province of Iran was investigated. GOSP flare is located at the South and North Oil and Gas Separation Plants (N-GOSP and S-GOSP) at the South Azadegan oilfield, about 2 km west of Ahvaz.

The flare consists of a three-sided derrick structure with a height of 46 m that supports a stack with a height of 51 m. The derrick structure consists of a three-sided concentrically braced steel frame. The column arrangement for EL 0.08 (the top of the base plate) is for a radius of 4.5 m. The columns incline upward to EL+34 in an arrangement with a radius of 2.75 m. The frame elevation was considered for EL +8.0, +16.0, +22.0, +28.0, +34, +38.0, +42.0 and +46.0. The stack was restrained at these elevations in the horizontal direction and was free in the Z direction.

The GOSP flare is denoted as FL-01-3S-H51 in which FL is flare, 01 is the case study number, 3S indicates that it is three-sided and H51 is the height of the flare. The specifications of the sections [18] and materials used for modeling are shown in Table 2 and Table 3, respectively. Their geometry is shown in Fig. 2.

Table 2
Section Properties for FL-01-3S-H51.

Element	Section	Diameter (mm)	Thickness (mm)
Column	Pipe-14"	355.6	9.53
	Pipe-14"	355.6	7.12
	Pipe-14"	355.6	6.35
Beam and brace	Pipe-12"	323.8	6.35
	Pipe-8"	219.1	6.35
	Pipe-6"	168	6.35

Table 3
Material Properties of FL-01-3S-H51.

Element	Material	Elasticity module (kg/m2)	Poisson ratio	Yield stress (kg/m2)	Ultimate stress (kg/m2)	Mass density (kg/m3)
Stack shell	ASTM 10^6 Gr B	2.038×10^{10}	0.3	24000000	41500000	7849
Pipe for derrick	ST-37	2.038×10^{10}	0.3	24473189	36709780	7849

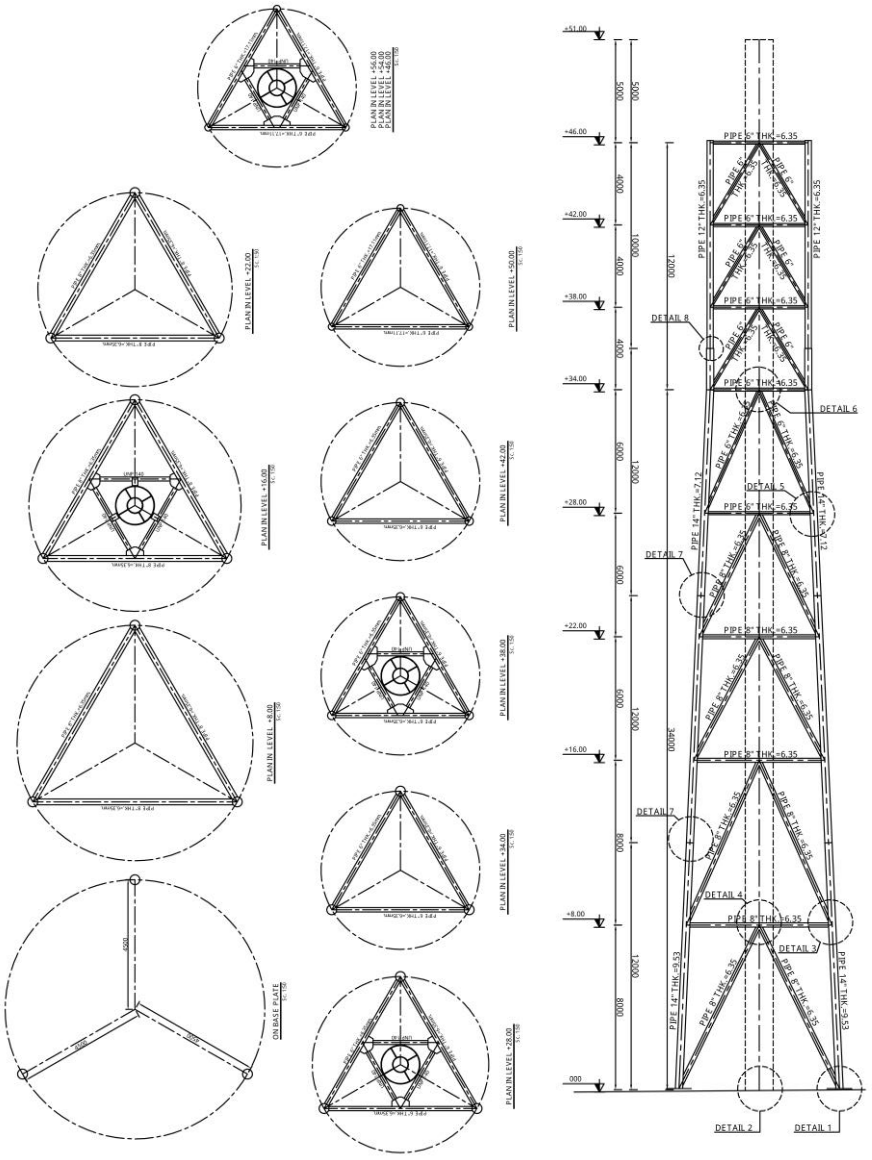

Fig. 2. Elevation Levels and Sections.

Based on the information and explanations given above regarding the geometric properties of the materials, the analysis and design of the structure was done using 3D mathematical modeling in SAP2000 (ver. 14.2.2). The nature of the structural trusses, the articulated coupling of the beams and braces and the type of truss system used resulted in a low moment in the columns. Thus, it

was not possible to form bending plastic hinges in the members so that the structural plastic hinges were axial in the center of the columns and braces according to FEMA 356 [13]. Fig. 3 is a finite element model of the structure.

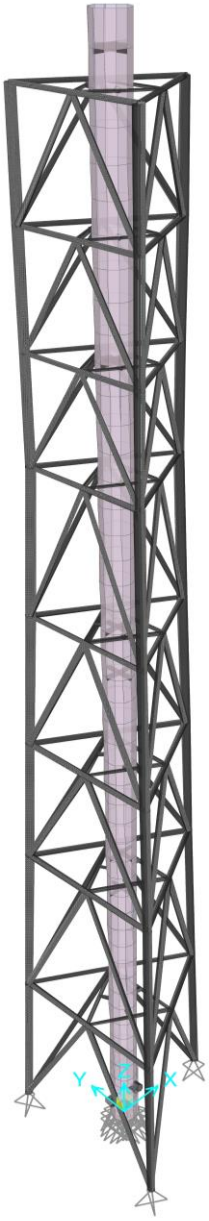

Fig. 3. Modeled Structure.

Table 4
Mode Results.

MODE	T	Ux	Uy	Uz
1	0.81919	0.45419	0.13799	0.0000012
2	0.81818	0.13804	0.454165	0.000123
3	0.25602	0.00529	0.00093	7.793E-09

It is worth noting that all the connections of the members, as well as the connection of the stack and derrick to the ground, were articulated coupling. The loads applied to the derricks are based on ASCE 7-10 [13] criteria and the coefficients and the basics provided in the manufacturer technical specifications for the flare package are as follows:

Load applied to the substructure:

- Dead Load
- Live Load
- Ambient temperature
- Operational temperature due to flaring
- Wind load
- Seismic load

Dead loads include the self-weight of the structure and all the attachments that support the structures. Other fixtures and all attachments, including the access ladder load, platforms and tip flaring, should be assigned to the structure. A thermal uniform variation of ±30°C was assigned to structure. A thermal uniform variation of from 250°C at top of the flare to 100°C at the base were assigned to the structure. The wind load was calculated according to ASCE07-10, section 29.5. The period of the structure for the first three modes is given in Table 4.

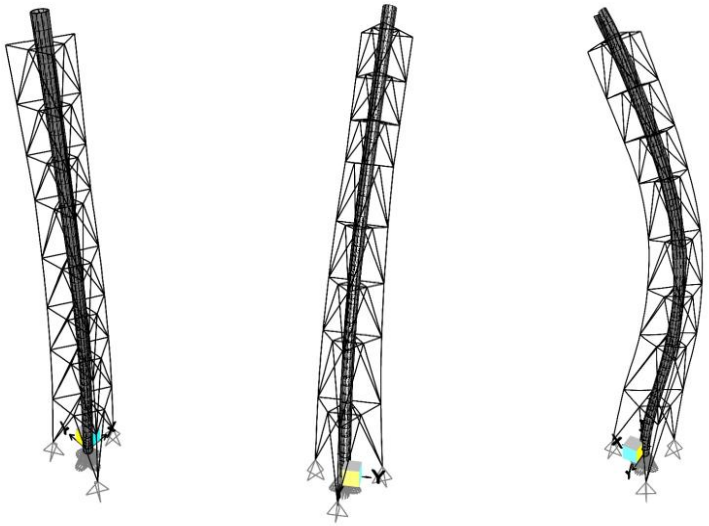

Fig. 4. First Three Modes Shapes.

5. Ground motion set selection

In many seismic studies, accelerograms are based on the characteristics of the study area, such as the distance from the fault, the magnitude, the type of soil, and other source-related parameters so that are most similar to potential accelerograms in the region. The selected accelerograms are scaled to the desired level for seismic studies. For IDA, however, studies show that there is no need for high sensitivity in the choice of accelerometers based on distance and magnitude because there is little difference in the results [19].

Cornell [15] recommended the use of 10 to 20 earthquake records as being reasonably accurate for estimating damage demand. Fifteen accelerograms were extracted from the PEER [13] earthquake database for the present study. Their characteristics are shown in Table 5. Their response spectra using the Jennings [20] numerical method in scaled and unscaled form are shown in Fig. 5 and Fig. 6, respectively.

Table 5
Selected Ground Motions.

No.	Event	Station	ϕ	Year	Soil	M	R	PGA
1	Imperial Valley	Plaster City	135	1979	III	6.5	30.33	0.058
2	Loma Prieta	Hollister Differential Array	255	1989	III	6.9	24.82	0.279
3	Loma Prieta	Coyote Lake Dam (Downst)	285	1989	III	6.9	20.8	0.179
4	Imperial Valley	El Centro Array #13	140	1979	III	6.5	21.98	0.118
5	Loma Prieta	Sunnyvale Colton Ave	270	1989	III	6.9	24.23	0.207
6	Superstition Hills	Wildlife Liquefaction Array	360	1987	III	6.5	23.85	0.208
7	Loma Prieta	Hollister South & Pine	000	1989	III	6.9	27.93	0.37
8	Imperial Valley	Plaster City	045	1979	III	6.5	30.33	0.043
9	Loma Prieta	Hollister Differential Array	165	1989	III	6.9	24.82	0.269
10	Imperial Valley	El Centro Array #13	230	1979	III	6.5	21.98	0.139
11	Loma Prieta	Sunnyvale Colton Ave	360	1989	III	6.9	24.23	0.207
12	Northern Calif	Ferndale City Hall	044	1954	III	6.5	27.02	0.163
13	San Fernando	LA - Hollywood Stor FF	090	1971	III	6.6	22.77	0.225
14	Imperial Valley	Calipatria Fire Station	225	1979	III	6.5	24.6	0.129
15	Loma Prieta	Agnews State Hospital	090	1989	III	6.9	24.57	0.161

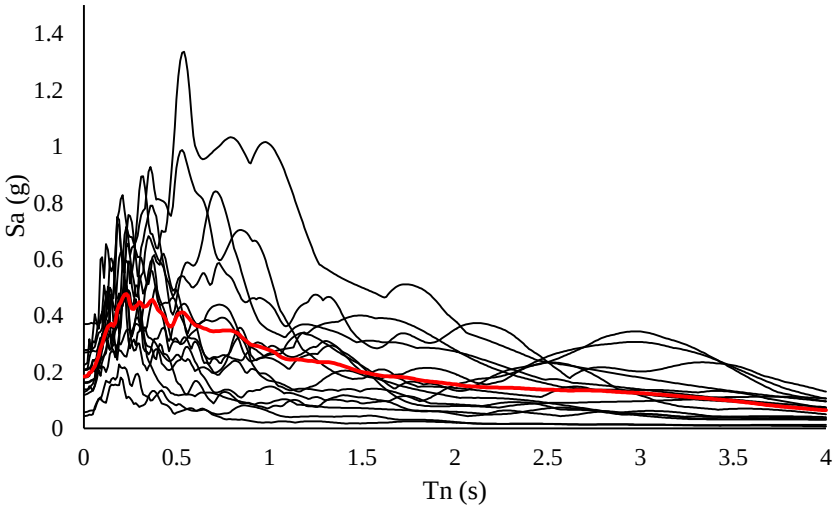

Fig. 5. Non-Scaled Pseudo-Acceleration Response Spectrum with 5% Damping Ratio.

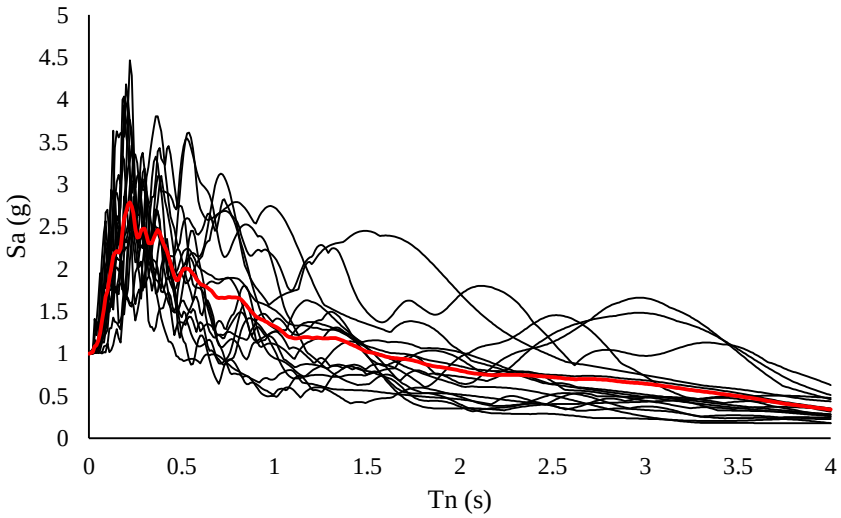

Fig. 6. Scaled Pseudo-Acceleration Response Spectrum at 5% Damping Ratio.

6. IDA results

The behavior of structures under the influence of 15 records was investigated separately for the longitudinal and transverse directions using IDA. The data obtained for each accelerometer as discrete points for structural damage (DM) versus scaled seismic intensity (IM) have been plotted in IDA curves. For this purpose, using the Interaction ability of SAP2000 with VBA (Visual Basic Application) a fully automatic program is provided for IDA analysis and exporting the results, that is necessary for IDA analysis because of numerous analysis to preventing manual errors.

In Fig. 7 through IDA Curves in Longitudinal Direction. these results are plotted as the maximum intersegment displacement ratio (ISDR $_{max}$) versus PGA.

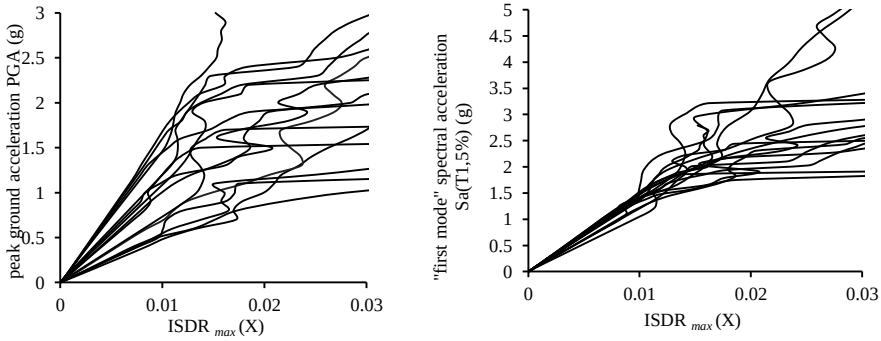

Fig. 7. IDA Curves in Longitudinal Direction.

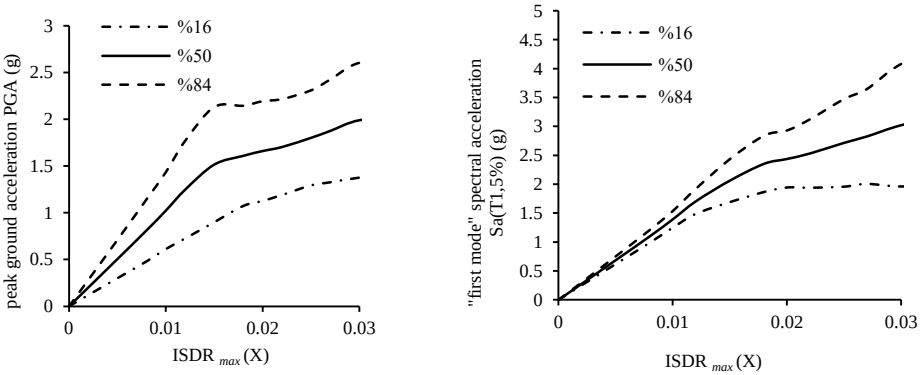

Fig. 8. Simplified IDA Curves in Longitudinal Direction.

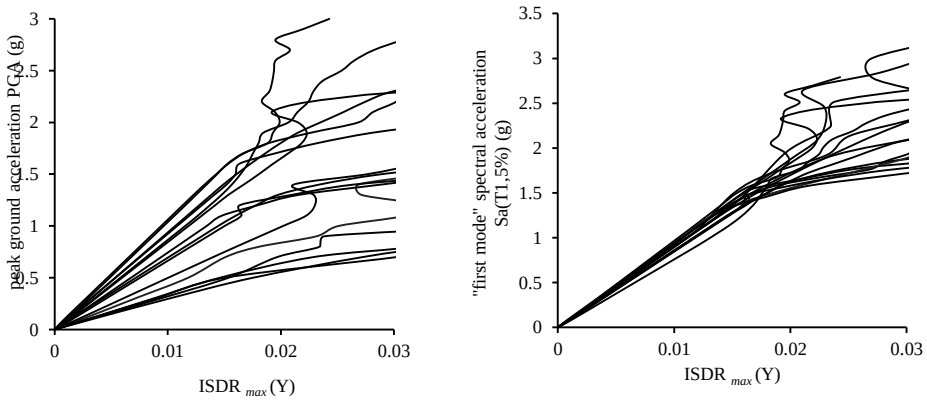

Fig. 9. IDA Curves in Transverse Direction.

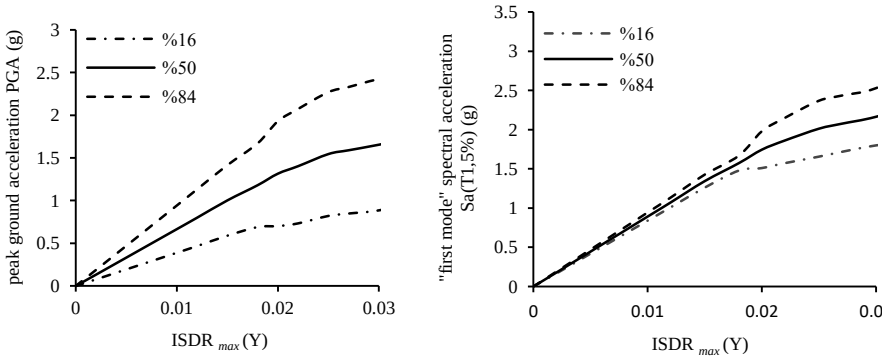

Fig. 10. Simplified IDA Curves in Transverse Direction.

A fragility curve can be used to assess seismic vulnerability to earthquakes. The equations and explanations presented in the IDA section above and the three performance levels (IO, LS, CP) from FEMA 356 (Table 1) for the structures under consideration were used to evaluate the

probability of exceeding a specific damage state for a prescribed level of ground motion intensity by fitting the lognormal distribution to the data. The fragility parameters (CDF) and fragility curves are presented for the three damage levels in both the *x* and *y* directions. The probability values for each performance level shown in Table 6 and Table 7 and the fragility curves shown in Fig. 11 and Fig. 12 can be used as criteria for comparing the performance of similar structures.

Table 6
Lognormal Parameters of Fragility Curves in Longitudinal Direction.

Damage state	Median (g)	Standard deviation
I	0.41	0.40
II	1.21	0.37
III	1.48	0.37

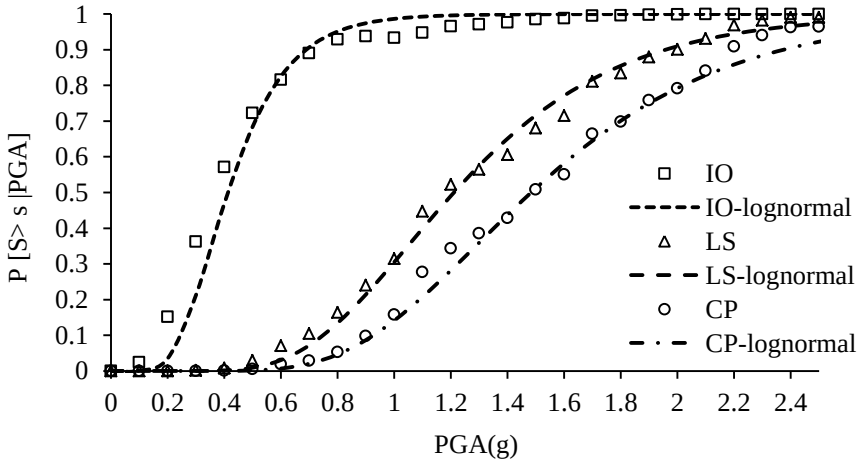

Fig. 11. Fragility Curves for Longitudinal Direction.

Table 7
Lognormal Parameters of Fragility Curves for Cross Direction.

Damage state	Median (g)	Standard deviation
I	0.32	0.50
II	0.89	0.43
III	1.07	0.41

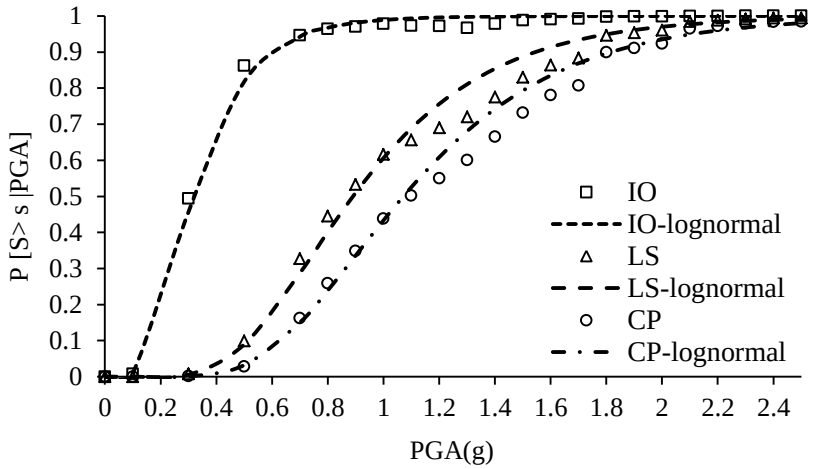

Fig. 12. Fragility Curves in Cross Direction.

7. Conclusion

The present study undertook a probabilistic seismic evaluation of derrick-supported flares. For this purpose, fragility curves were estimated using the probabilistic method and the related parameters are presented. The case study of a flare structure consisted of a three-sided derrick-type structure with a height of 46 m that supports a stack with a height of 51 m. The distribution of the damage index at each earthquake intensity was obtained using nonlinear IDA under the influence of 15 ground motion records extracted from the PEER site. The EDP was selected as the maximum intersegment displacement ratio and PGA was selected as the IM. The limit states were based on the damage levels from the FEMA 356.

An overview of the seismic safety results for these structures indicated very low probability values (for the LS and CP limit states) for an earthquake of up to 0.8g. The earthquake probability for the area is 0.35g with a very low probability of exceeding the IO limit state for earthquakes up to 0.4g. The seismic requirements of such structures are not high for ordinary seismic intensity measures, although it is recommended to apply seismic codes regulations to prepare for rare earthquakes.

The results for the prevailing wind load for the design of these structures corresponded to available reports; thus, it can be said that the seismic requirements for these structures were not significant. The need for seismic evaluations for different types of flare structures and comparisons of the results with the fragility parameters is recommended.

References

[1] Di Sarno L, Karagiannakis G. On the seismic fragility of pipe rack—piping systems considering soil–structure interaction. Bull Earthq Eng 2020;18:2723–57. doi:10.1007/s10518-020-00797-0.

[2] Karimimalayer M. Evaluation on Capability of a Power Supply Company to Improve Environmental Management Systems According to Sustain Implementation of ISO 14001. Ind Eng Strateg Manag 2019;1:1–14. doi:10.22115/iesm.2019.87495.

[3] Caputo AC, Vigna A. Numerical Simulation of Seismic Risk and Loss Propagation Effects in Process Plants: An Oil Refinery Case Study. Vol 8 Seism Eng, 2017. doi:10.1115/PVP2017-65465.

[4] Eidinger JM. FRAGILITY OF NON-STRUCTURAL COMPONENTS FOR FEMA BENEFIT COST ANALYSIS. n.d.

[5] Rodolfo José Danesi Supervisors B, Bazzurro P, Vamvatsikos D. Seismic Risk of Industrial Plants: Assessment of a Petrochemical Piperack Using Incremental Dynamic Analysis 2015.

[6] Bursi OS, Paolacci F, Reza MS. Performance-Based Analysis of Coupled Support Structures and Piping Systems Subject to Seismic Loading. Vol 8 Seism Eng, 2015. doi:10.1115/PVP2015-45123.

[7] South Durban Community Environmental Alliance. Flaring at oil refineries in south Durban and Denmark. SDCEA; 2005.

[8] Svensson B. Global Gas Flaring Reduction 2004:24.

[9] American Petroleum Institute. Pressure-relieving and Depressuring Systems: API STANDARD 521 2014:260.

[10] Sabry H, Dhabi A. SPE-188307-MS Integrity of LNG Flare Systems. 2017.

[11] Papas M, Smith S, Zink D, Palfreeman N. Principals of flaring combustion and ways to minimize emissions and smoke design and case study of a new air injection system for upgrading exisiting flares into smokeless flaring. Soc Pet Eng - SPE Asia Pacific Oil Gas Conf Exhib 2010, APOGCE 2010 2010;3:1689–713. doi:10.2118/134067-ms.

[12] Akeredolu FA, Sonibare JA. A review of the usefulness of gas flares in air pollution control. Manag Environ Qual An Int J 2004;15:574–83. doi:10.1108/14777830410560674.

[13] Krausmann E, Cruz AM, Affeltranger B. The impact of the 12 May 2008 Wenchuan earthquake on industrial facilities. J Loss Prev Process Ind 2010;23:242–8. doi:10.1016/j.jlp.2009.10.004.

[14] Vamvatsikos D, Cornell CA. Incremental dynamic analysis. Earthq Eng Struct Dyn 2002;31:491–514. doi:10.1002/eqe.141.

[15] Vamvatsikos D. Seismic Performance, Capacity and Reliability of Structures as Seen Through Incremental Dynamic Analysis 2005:1–172.

[16] Etli S, Güneyisi EM. Seismic performance evaluation of regular and irregular composite moment resisting frames. Lat Am J Solids Struct 2020;17:1–22. doi:10.1590/1679-78255969.

[17] Chiou J-S, Chiang C-H, Yang H-H, Hsu S-Y. Developing fragility curves for a pile-supported wharf. Soil Dyn Earthq Eng 2011;31:830–40. doi:10.1016/j.soildyn.2011.01.011.

[18] Kumar P, Pandey S, Maiti PR. A modified genetic algorithm in c++ for optimization of steel truss structures. J Soft Comput Civ Eng 2021;5:95–108. doi:10.22115/SCCE.2021.242552.1249.

[19] Iervolino I, Cornell CA. Record selection for nonlinear seismic analysis of structures. Earthq Spectra 2005;21:685–713. doi:10.1193/1.1990199.

[20] Chopra AK. Dynamics of structures: theory and applications to earthquake engineering. Dyn Struct Theory Appl to Earthq Eng 2012. doi:10.1002/9781118599792.